Osteoarthritis and Cartilage Open xxx (xxxx) xxx

Contents lists available at ScienceDirect

Osteoarthritis and Cartilage Open

journal homepage: www.elsevier.com/journals/osteoarthritis-and-cartilage-open/2665-9131

The zonal evolution of collagen-network morphology quantified in early osteoarthritic grades of human cartilage

Phoebe Szarek [a], Magnus B. Lilledahl [b], Nancy C. Emery [c], Courtland G. Lewis [d], David M. Pierce [a,e,*]

[a] Department of Biomedical Engineering, University of Connecticut, Storrs, CT, USA
[b] Department of Physics, Norwegian University of Science and Technology, Trondheim, NOR, USA
[c] Department of Ecology and Evolutionary Biology, University of Colorado, Boulder, CO, USA
[d] Bone & Joint Institute, Hartford Healthcare, Hartford, CT, USA
[e] Department of Mechanical Engineering, University of Connecticut, Storrs, CT, USA

ARTICLE INFO

Keywords:
Cartilage
Osteoarthritis
Collagen network
Fiber orientation
Transmission electron microscopy

SUMMARY

Objective: We aimed to directly quantify the zone-specific evolution in morphology of collagen fibers and networks in human cartilage during the progression of early osteoarthritis. Collagen fibers exhibit depth-dependent orientations and diameters crucial to their mechanical roles. Cartilage degenerates in osteoarthritis, affecting the morphology of the collagen network and ultimately the intra-tissue mechanics.

Design: We obtained specimens of human cartilage from healthy human knees ($n = 3$) and from total knee arthroplasties ($n = 5$). We utilized TEM and custom image analyses to visualize and quantify distributions in principal orientation, dispersion (about the principal orientation), and diameter of collagen fibers in the early grades of OA within each through-thickness zone. We then used histological and statistical analyses to probe for significant changes in the zone-specific evolution in collagen-network morphology as a function of Osteoarthritis Research Society International (OARSI) grade.

Results: Dispersion in the alignment of collagen fibers increased with progression of early OA in both the superficial and deep zones, and decreased in the middle zone, while principal orientation did not change significantly. The non-normal and right-skewed distributions in fiber diameters did not evolve with the progression of OA.

Conclusions: We provide the research community with *quantitative* data (1) on the through-thickness morphology of collagen in healthy cartilage and (2) on the evolution of through-thickness morphology of collagen with progressing early OA. Such quantitative data facilitate an improved mechanistic understanding of the progression of OA, and may facilitate identifying image-based biomarkers and treatment targets, and ultimately finding clinical interventions for OA.

1. Introduction

The remarkable mechanics of articular cartilage derive from complex interactions of charged proteoglycans, collagens, and electrolytic fluid [1,2]. In healthy, human cartilage collagen fibers constitute approximately 60% of the dry weight [3] and create a network with important contributions to overall mechanical strength and stiffness [4], e.g. collagen density strongly correlates with local shear modulus [5]. In health these fibers form a network that exhibits depth-dependent principal orientations and distributions in diameters: fibers in the superficial zone (SZ) have the smallest diameters and generally align with the articular surface, fibers in the deep zone (DZ) have the largest diameters and align perpendicular to the cartilage-bone interface, and fibers in the middle zone (MZ) create a transition between these two morphologies with either a random/isotropic alignment [6] or a gradual realignment of orientation as in the Benninghoff model [7].

The depth-dependent morphology of collagen fibers creates specific intra-tissue mechanics and functions in cartilage that deteriorate in osteoarthritis (OA), a disease of the synovial joint, with degeneration and loss of articular cartilage as one hallmark change. In healthy cartilage strong alignment of fibers (to the articular surface) in the SZ, e.g. creates a low-friction, tensile-resistant surface layer, while fibers within the DZ

* Corresponding author. Department of Mechanical Engineering, University of Connecticut, 191 Auditorium Road, Storrs, CT, 06269, United States.
E-mail address: dmpierce@engr.uconn.edu (D.M. Pierce).

https://doi.org/10.1016/j.ocarto.2020.100086
Received 8 May 2020; Accepted 14 July 2020

anchor cartilage to the subchondral bone and provide shear stiffness [8,9]. The average diameter of collagen fibers also correlates with the ultimate tensile strength across many connective tissues [4]. In late OA microstructural changes in the collagen network of articular cartilage alter recruitment of fibers under applied loads [10]. Changes in the diameters of fibers, and the inter-fibril spacing, likely also impact permeability and inter-constituent interactions [11]. Qualitatively, the loss of volume and microstructural organization produces a less resilient cartilage unable to perform its *in vivo* mechanical role.

Previous studies applied different imaging modalities and image-analysis methods to probe morphology of collagen fibers and networks in biological tissues. *Ex-vivo* modalities for imaging cartilage include Polarized Light (PLM), Second Harmonic Generation (SHG), Scanning Electron (SEM), and Transmission Electron Microscopy (TEM) [12–15]. Pixel-wise methods for image analyses relate each pixel to a skeletonized binary representation or use vector summations of pixel intensity and position [16,17]. Alternatively, Fourier transformations facilitate detection of orientation in images of many fibrous tissues including ligament, cornea/sclera, arteries, and cartilage [18–23]. These methods may include additional filtering in either the spatial (e.g. Gaussian filters) or the frequency (e.g. bandpass and wedge filtering) domains, or sampling based on fiber-dimensions [19,20,22,24]. Each approach has benefits and drawbacks that depend on the research questions.

Previous studies report that osteoarthritic articular cartilage presents both a range of localized OA severity within individual joints [25,26] and corresponding changes within the network of collagen. The principal orientation and dispersion of collagen fibers in human patellar cartilage, visualized via PLM, showed significant changes with advanced OA [13]. OA-induced damage also caused the orientation of collagen to become more dispersed (less well aligned) throughout bovine metacarpophalangeal cartilage (10). Comparison of healthy versus degraded human cartilage, visualized by PLM, showed an increase in fiber disorganization and a corresponding decrease in fiber diameters [27]. Unfortunately the authors used only qualitative measures and compared healthy cartilage from the knee to degraded cartilage from the hip. Thicker collagen fibers of osteoarthritic human knee and hip cartilage also appear to unwind into thinner fibers, as noted in SEM images [15]. Nonetheless, no results quantify the progression of collagen network morphology from direct fiber measurements at multiple points during progression of early grades of OA using human cartilage from the same joint. In this study we aimed to directly quantify the zone-specific evolution in morphology of collagen fibers and networks in human cartilage with advancing histological grade of OA, hereafter defined as progression of OA. We utilized TEM and custom image analyses to visualize and quantify distributions in principal orientation, dispersion (about the principal orientation), and diameter of collagen fibers in early OA within each through-thickness zone. We then used histological and statistical analyses to test for significant zone-specific changes as a function of Osteoarthritis Research Society International (OARSI) grade [28]. Quantitative longitudinal data on the zone-specific morphology of collagen may elucidate evolving bulk- and intra-tissue mechanics intimately connected to the degenerative progression of OA, facilitate identifying new biomarkers for disease progression, and aid modeling of OA-associated matrix degradation.

2. Materials & methods

2.1. Preparation of specimens

We obtained specimens from femoral condyles of healthy human knees from the Musculoskeletal Transplant Foundation ($n = 3$) and from cartilage removed during total knee arthroplasties at Hartford Healthcare Bone & Joint Institute ($n = 5$). A review by the Institutional Review Board (IRB, Assurance #FWA 00000601) found that this study did not constitute research involving human subjects according to 45 CFR 46.102(f) and therefore did not require further review or oversight by the IRB. We stored specimens at − 80°C in phosphate-buffered saline [29]. We determined the local split-line direction (SLD) by pricking the articular surface with a dissecting needle dipped in India ink [30]. We extracted 30 pairs of 3 mm by 3 mm, full-thickness (≈ 4 − 5 mm) cuboid specimens of cartilage using razor and surgical scalpel blades with one though-thickness edge parallel to the SLD. We extracted multiple pairs of specimens from presumed load-bearing regions of the medial or lateral condyle from each patient. From each pair of specimens we used one specimen for histological assessment (Section 2.2) and reserved the other for TEM (Section 2.3). Fig. 1 outlines our process for gathering quantitative information from each source of cartilage.

2.2. Histological assessments

We fixed specimens in 10% neutral buffered formalin and decalcified them in 0.5 M EDTA before embedding in paraffin and sectioning. We stained each section with Safranin O fast green (Novaultra Safranin-O stain kit, IHC World, Ellicott City, MD). Four trained research scientists independently graded randomized histological images according to the OARSI grading system [28]. We averaged grades to obtain a single OARSI grade for each specimen characterizing the *local* severity of OA. After reviewing the source of each specimen and its histological assessment, we selected 18 cuboidal specimens across all patients and grades to process for TEM imaging (see Appendix B). We binned specimens into five groups based on grade: healthy (from healthy source, H), normal (grade <1, OA-0), early (1 ≤grade <2, OA-1), mild (2 ≤grade <3, OA-2), and moderate (3 ≤grade <3.5, OA-3).

2.3. Transmission electron microscopy

The day of fixation we thawed the specimens, trimmed off all subchondral bone, and cut the cuboids into 0.5 mm thick slices parallel to the SLD using a surgical scalpel. We placed each in a fixative composed of 3.0% glutaraldehyde, 3.0% paraformaldehyde, 0.05% w/v tannic acid in 0.1 M PIPES buffer overnight [31]. We performed post-fixation with 1% osmium tetroxide for one hour and en bloc staining with 2% uranyl acetate in 50% ethanol for 15 min and 2.5% Reynold's lead citrate for three minutes. We dehydrated and cleared the specimens in graded ethanol and in propylene oxide, respectively. We infiltrated and embedded the specimens with low-viscosity Spurr's resin and polymerized the resin in a flat-bottomed embedding capsule for 24 h at 70°C. We cut ultrathin (50 nm) sections using a Diatome Ultra 45° diamond knife (Diatome US, Hatfield, PA) on a Leica Ultracut UCT ultramicrotome (Leica Biosystems Inc., Buffalo Grove, IL) and collected sections on copper 100 mesh grids. We collected the top and bottom half of serial sections on separate grids in cases where through-thickness sections were larger than 2 mm. We stained all grids with 1.5% saturated uranyl acetate for ten minutes and 2.5% lead citrate for three minutes.

We imaged sections using a FEI Technai 12 G2 Spirit BioTWIN (FEI Company, Hillsboro, OR) at 80 kV with a four megapixel 2k XR40 CCD camera (Advanced Microscopy Techniques, Woburn, MA). We located both the articular surface and hyaline-calcified cartilage interface and measured total specimen thickness using the built-in navigation software. We calculated ten imaging locations equally spaced horizontally (parallel to the articular surface) at the vertical center of each zone using zonal definitions based on total thickness: Superficial–SZ (0–15%), Middle–MZ (15–70%), Deep–DZ (70–100%) [6]. In cases where the designated imaging location fell on a chondrocyte, grid bar, or processing artifact we moved the imaging location to the nearest unaffected region. We captured all images at 11,000× magnification.

2.4. Analyses of microscopy images

We used the articular surface and hyaline-calcified cartilage interface to find the relative orientation φ between these (roughly parallel) sur-

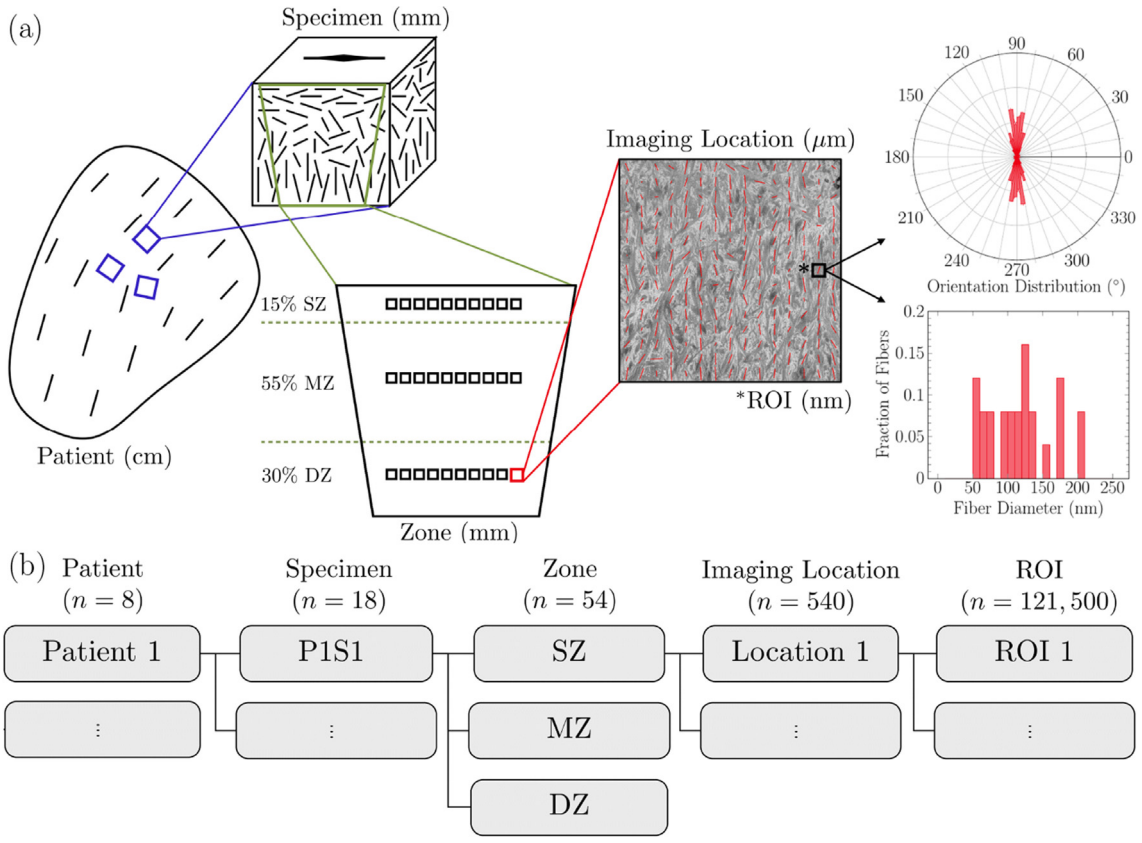

Fig. 1. Quantifying the through-thickness morphology of collagen in cartilage based on imaging of collagen fibers via transmission electron microscopy. (a) We extracted 3 mm by 3 mm, full-thickness cuboid specimens of cartilage from healthy patients and patients with OA. We then sectioned the specimens into 50 nm slices parallel to the local split-line direction for imaging via transmission electron microscopy at ten locations parallel to the articular surface in each of three through-thickness zones (superficial, middle, and deep). We analyzed each image by dividing it into smaller regions of interest (ROIs) to obtain data on the orientation and diameter of fibers. (b) Starting from $n = 8$ patients, we analyzed data from a total of $n = 18$ specimens. Within each specimen, we quantified the network of collagen in each of the three through-thickness zones to obtain parameters characterizing each of the $n = 54$ specimen-zone groups. We used these parameters in ANCOVA analyses of zone-, grade-, zone-grade-, patient-, and specimen-effects, and calculated these by averaging data collected at the $n = 225$ ROIs from each of the $n = 10$ imaging locations within each zone.

faces and the coordinate axes used in TEM imaging. We divided each image into square regions of interest (ROIs) and determined the principal orientation for every ROI. In a preliminary study we ran the analysis within a reasonable range of ROI sizes (see Appendix A) and finally used a ROI size of 120 × 120 pixels, equivalent to ~650 × 650 nm or 15-by-15 ROIs per image. We transformed each ROI into the Fourier domain. Given the Fourier transform of the image $P(u,v)$, we analytically minimized the function (Eq. 1)

$$f(\alpha_i) = \sum_u \sum_v |P(u,v)| \sin^2(u,v,\alpha_i), \tag{1}$$

where (u,v) is a point in the Fourier image and α_i is the principal direction (angle) for a given region [19].

For each ROI, we considered the principal direction as a unit vector with direction α_i. We used the relative orientation φ of the section to rotate the principal direction back into a common configuration using the articular surface as a reference (zero degrees or horizontal). We bounded the principal directions (angles) to $\alpha_i \in [0,\pi)$ to account for undirectional fibers, and multiplied each angle by two to account for central symmetry [32]. We calculated the mean vector $(\overline{\alpha}, r)$ characterizing the circular fiber distribution using (Eqs. 2–4)

$$c = \frac{1}{n}\sum_{i=1}^{n} \cos(\alpha_i), \tag{2}$$

$$s = \frac{1}{n}\sum_{i=1}^{n} \sin(\alpha_i), \tag{3}$$

$$r = \sqrt{c^2 + s^2}, \tag{4}$$

where n is the total number of ROIs and directions α_i within a specific image, i.e. $n = 225$, and (Eq. 5)

$$\overline{\alpha} = \begin{cases} \tan^{-1}\left(\frac{c}{r}\right), & \text{if } c \geq 0, \\ \tan^{-1}\left(\frac{c}{r}\right) + \pi, & \text{if } c < 0, \end{cases} \tag{5}$$

where $\overline{\alpha} \in [0, 2\pi)$ is twice the mean direction within an image and $r \in [0,1]$ measures the corresponding dispersion (strength of alignment in direction $\overline{\alpha}$ or lack thereof) with $r = 0$ indicating uniform isotropy and $r = 1$ indicating perfect alignment.

To facilitate comparisons with prior literature, e.g. Ref. [20,21], we determined parameters θ and κ from the π-periodic von Mises circular normal distribution (Eq. 6)

$$f(\alpha) = \frac{1}{\pi I_0(\kappa)} e^{\kappa \cos(2(\alpha-\theta))}, \tag{6}$$

where $I_0(\kappa)$ is the modified Bessel function of the first kind of order zero and κ is a concentration parameter that characterizes dispersion about the principal orientation θ. We determined $\theta \in [0,\pi)$ by dividing the

mean direction $\overline{\alpha}$ by two (again accounting for central symmetry) and we determined κ from the measure of dispersion r as [33] (Eq. 7)

$$\kappa=\begin{cases}2r+r^3+5r^5/6, & \text{if } r<0.53,\\ -0.4+1.39r+0.43/(1-r), & \text{if } 0.53\leq r<0.85,\\ 1/\left(r^3-4r^2+3r\right), & \text{if } r\geq 0.85.\end{cases} \quad (7)$$

The concentration parameter $\kappa\in[0,\infty)$ quantifies the distribution in principal orientation with $\kappa=0$ for uniform (isotropy) and $\kappa=\infty$ for perfectly aligned (Dirac delta). We implemented our analyses in Matlab (R2019a, The MathWorks, Natick, USA).

We also generated a 5-by-5 even grid over each image and measured the diameter of the fiber closest to the center of each region using ImageJ [34]. Thus we measured the diameter of $n = 25$ fibers while minimizing subjectivity.

2.5. Statistical analyses

We selected specimens allowing us to assess inter-grade and inter-patient variability in the morphology of the networks of collagen. We processed specimens until we obtained sufficient power ($\beta > 0.80$) in post-hoc analysis of the zone-grade effect on the mean value of κ. We used the Rayleigh test to check for uniform fiber orientation distributions within all zones of all specimens. We calculated the specimen mean and specimen standard deviation (M±SD) of each parameter (θ and κ) for each zone within each specimen, using the parameters from the $n = 10$ images in the zone and assuming normality. We used a Shapiro-Wilks test to check for normality in our data on the diameter of fibers. We analyzed normally distributed data on fiber diameter using M±SD and non-normally distributed data using median and interquartile range (M + IQR). We determined mean and 95% confidence interval (M±95%CI) of all parameters in each zone in each grade using mean values from the $n = 3-6$ specimens within each grade, assuming normally distributed measurements within a grade-zone.

We used nested, mixed-model ANCOVAs assuming homoscedasticity to evaluate how the morphology of the networks of collagen varied among zones and grades. We completed a separate analysis for each of the six response variables: mean principal orientation θ, SD of principal orientation θ, mean concentration parameter κ, SD of concentration parameter κ, median fiber diameter, and IQR of fiber diameter. We treated zone as a fixed categorical effect, grade as a continuous variable, and patient as a random effect. We included the interaction between zone and grade, and accounted for non-independence among specimens extracted from the same patient by nesting specimen within patient. We further evaluated statistically significant effects of zone and grade using post-hoc, Tukey-Kramer tests with corrections for multiple comparisons. The standard deviation of κ was $\log(x+0.01)$ transformed to meet the assumptions of ANOVA but the five other response variables met model assumptions without transformation. We used SAS 9.4 (Cary, NC) for these analyses and reported the degrees-of-freedom df, F-ratio F, p-value, and model-estimated parameters as least-square estimates plus or minus standard error (LSE±SE).

Using relative zonal comparisons within each specimen (e.g. SZ<MZ and DZ for fiber diameters), we used a proportion test to identify specimen-independent, relative zonal characteristics. To probe changes in the diameters of fibers across grades, e.g. the number of large (≥ 200 nm) fibers, we used a Student's t-test. To assess inter-observer agreement in OARSI grading, we calculated Fleiss's kappa coefficient κ_F. We used a threshold of $\alpha = 0.05$ for statistical significance, but we illustrated effect sizes and report key statistical parameters (e.g. degrees of freedom, F statistics, and P-values) that support our primary conclusions to avoid confounding statistical significance and scientific relevance [35].

3. Results

We analyzed 540 images from TEM and from each obtained 225 measurements of mean direction and dispersion, and 25 measurements of fiber diameter. Fig. 2 and Fig. D6 show representative results from a cartilage specimens of Grade 0 and Grade 3, respectively.

We found fair inter-observer agreement ($\kappa_F = 0.292$) in OARSI grading of cartilage specimens by four individuals.

3.1. Overall collagen morphology

We observed substantial variation among zones in all six response variables longitudinally, from healthy to OARSI grade 3. Specifically, the mean principal orientation varied among zones ($df = 2,32; F = 12.35; p < 0.001$), though post-hoc tests revealed that the small mean principal orientation θ within the SZ (0.19 ± 0.14) relative to both the DZ (1.33 ± 0.14) and the MZ (1.17 ± 0.14), which were not significantly different from one another, drove this effect. Similarly, the large estimate in the SZ (3.19 ± 0.39) relative to the DZ (1.67 ± 0.39) and MZ (1.19 ± 0.39), which were not significantly different from one another, drove variation in the mean of concentration parameter ($df = 2,32; F = 12.18; p < 0.001$). The difference between the SZ and MZ, which were individually not significantly different from the DZ, drove the variation in the SD of θ and κ ($df = 32; t = 3.48; p = 0.004$ and $df = 36; t = -3.15; p = 0.009$, respectively). Post-hoc tests revealed that median and IQR of fiber diameter were significantly different among all zones.

We found no uniform distributions in principal orientations of collagen fibers when grouping data by zone, grade, or zone-grade. Using the mean concentration parameter κ as a measure of dispersion, fibers were the most aligned in the SZ in 12 out of the 18 specimens ($z = 3.09$; $p = 0.002$). All distributions of diameters of fibers were non-normal and right skewed for each zone-grade. The median diameter of collagen fibers was smallest in the SZ in 15 out of 18 specimens ($z = 4.54; p < 0.001$) and was largest in the DZ in 13 out of 18 specimens ($z = 3.52; p < 0.001$).

3.2. Evolution of collagen morphology

Fig. 3(a) shows the evolution of mean principal orientation and of von Mises concentration parameter (as a measure of dispersion in orientation) of collagen fibers in early grades of OA.

Neither the mean or standard deviation of the principal orientation ($df = 1,32; F = 1.90; p = 0.18$ and $df = 1,32; F = 2.64$, $p = 0.11$, respectively) changed with grade; this was consistent across zones ($df = 2,32; F = 1.56; p = 0.22$ and $df = 2,32; F = 0.43; p = 0.66$). We detected marginally significant tendency for mean concentration parameter κ to decline as grade increases ($df = 1,32; F = 3.68; p = 0.06$) and a relatively large interaction between grade and zone ($df = 2,32; F = 5.93; p = 0.007$). The mean concentration parameter decreased with progression of OA in the SZ while we did not detect significant changes in the MZ and DZ. Assuming a linear model, the estimated slope in the SZ and DZ equaled $-1.17 \pm 0.30$and -0.09 ± 0.43, respectively, while in the MZ this equaled 0.25 ± 0.43(see Appendix C). The standard deviation of κ did not vary substantially with grade ($df = 1,36; F = 0.04; p = 0.83$), but there is an interaction effect ($df = 2,36; F = 3.70; p = 0.03$).

Fig. 3(b) shows the evolution in the distributions of fiber diameters with grade and zone. The non-normal and right-skewed character of the distributions did not evolve with the progression of OA. Our analyses did not detect any statistically significant effect of grade, or the interaction between grade and zone on the distribution of fiber diameters (grade effect on median: $df = 1,32; F = 0.35; p = 0.56$; grade effect on IQR: $df = 1,32; F = 0.73; p = 0.40$; grade-zone interaction effect on median: $df = 2,32; F = 0.45; p = 0.64$; grade-zone interaction effect on IQR: $df = 2,32; F = 0.77; p = 0.47$). Past OARSI Grade 1, the number/fraction of larger fibers (≥ 200 nm) decreased nearly significantly ($df = 16;$

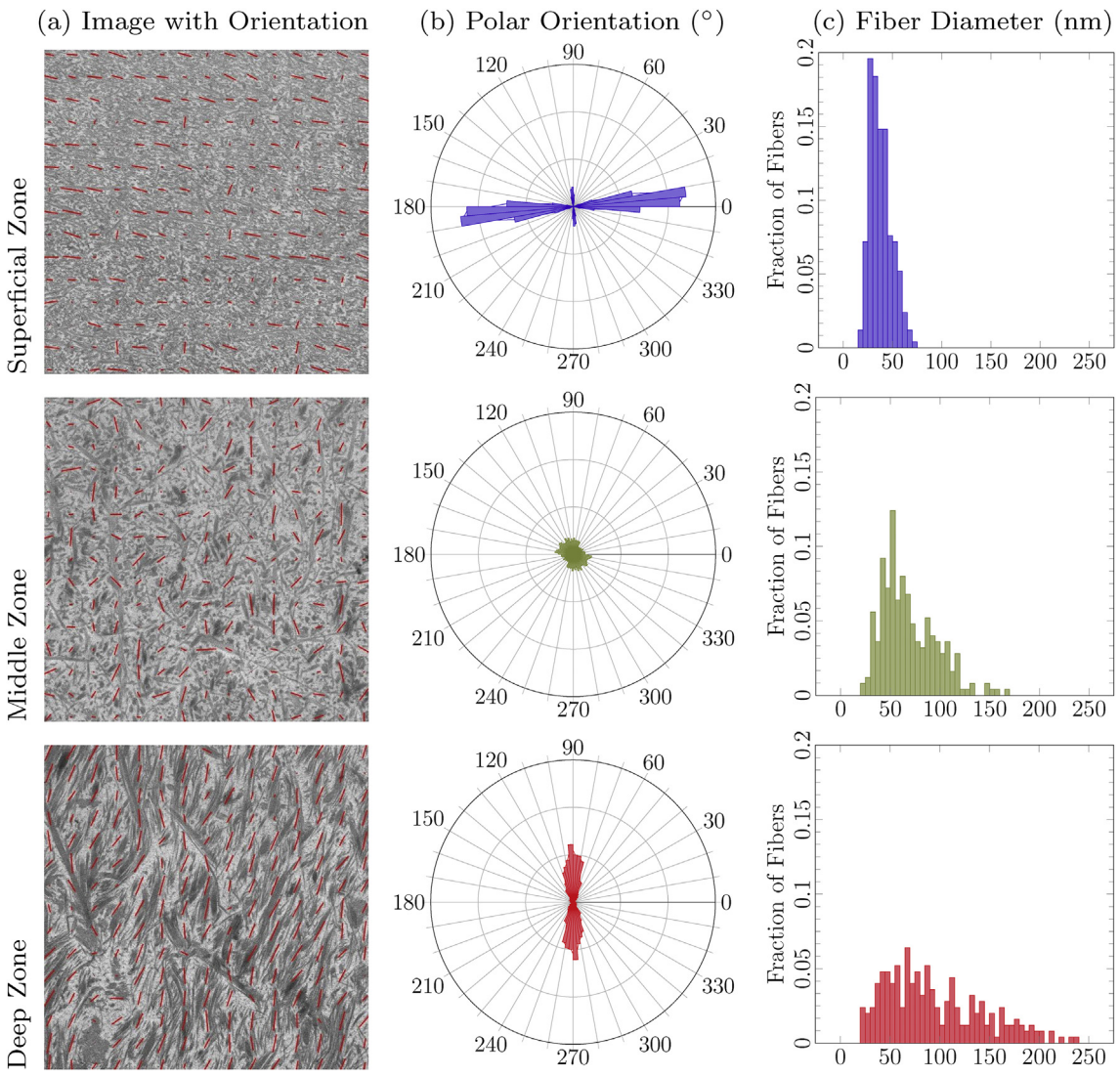

Fig. 2. Representative results from a cartilage specimen of Grade 0 show significant zonal differences in principal orientation, dispersion in orientation, and diameter of fibers, differences that generate through-thickness mechanical heterogeneity. (a) Zonal images from transmission electron microscope (width = 6 μm) each reveal a different distribution of local principal directions within 225 ROIs, each represented as red vectors. (b) Corresponding probability-normalized polar histogram of principal orientation presented. (c) Corresponding histogram of diameter of fibers.

$t = 1.73; p = 0.052$).

Table 1 provides the quantitative evolution of mean principal orientation θ, von Mises concentration parameter κ, and mean diameter plus IQR of collagen fibers in cartilage in health (H) and early grades of osteoarthritis (OA-0–OA-3), in the SZ, MZ, and DZ.

3.3. Inter- and intra-patient variability

We did not detect significant variation among patients in any of the response variables; in all models, the estimated variance for the random effect of patient was zero. While several models estimated non-zero variance among specimens (nested within patient), this variation was never statistically significantly different from zero (Z tests, $p > 0.25$ for all analyses).

4. Discussion

TEM imaging offers a valuable method to observe collagen networks in cartilage *ex vivo* because specimen preparation preserves the "hydrated," *in vivo*-like state. Any processing of soft tissues can affect the internal structures, and minimal isotropic shrinkage was a possible artifact of our process potentially affecting the measured fiber diameters. We captured images at a resolution of ≈5.4 nm per pixel, while we found almost no fibers with diameters less than 20 nm (< 0.2%). Other studies reported minimum fiber diameters of $10 - 38.6$nm, the largest possibly exaggerated by a coating of 5–10 nm of gold to faceplate imaging via SEM [27,36,37]. Hence our results fit within the expected range of minimum diameters, thus supporting our methods.

In analyzing our images to quantify fiber orientation and dispersion, we decided on a ROI size of $\sim 650 \times 650$ nm. Our ROI analyses capture the overall orientation of $\sim 3 - 15$ fibers while minimizing computational cost. A ROI size too large would mask local changes in fiber orientation and a size too small would be susceptible to noise and computationally expensive.

4.1. Overall collagen morphology

Our results on the overall morphology of the healthy collagen network are consistent with literature: in the SZ networks aligned with the articular surface while in the DZ networks aligned perpendicular to the cartilage-bone interface [38].

There is some discrepancy in the literature regarding the morphology

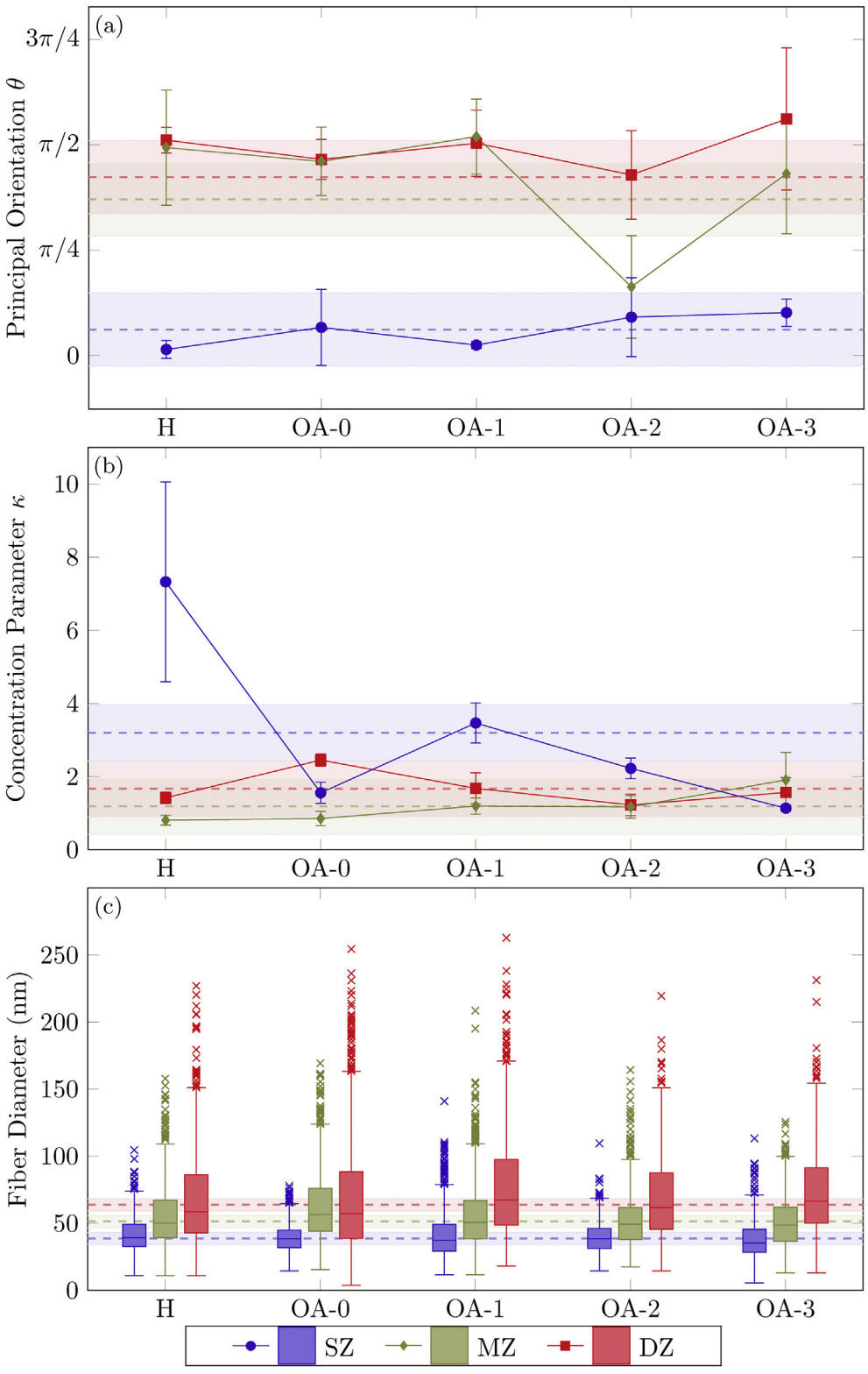

Fig. 3. In early osteoarthritis human cartilage exhibits significant changes in dispersion of collagen fibers but not principal orientation or diameter. Evolution of (a) the mean principal orientation θ and (b) the von Mises concentration parameter κ (as a measure of dispersion in orientation) of collagen fibers in cartilage in health (H) and in early grades of osteoarthritis (OA-0 – OA-3) in the superficial zone (SZ), middle zone (MZ), and deep zone (DZ). (c) Evolution of zone-specific distributions in diameters of fibers. We quantify these data for, e.g. mechanical modeling, in Table 1.

of the collagen network in the MZ. Some sources report that the MZ contains an effectively isotropic distribution in orientations, cf. [6,39]. Other sources report that fibers run continuously from the SZ through a transition then adopt an orientation perpendicular to the articulating surface through the MZ and DZ, cf. [7,10,40], an architecture commonly called the Benninghoff arcade model. Our results in the MZ also presented some alignment ($\kappa > 0$) with a principal orientation five times closer ($\geq 25\times$ closer before Grade 2) to the principal orientation of the DZ than that of the SZ. The increase in fiber alignment, and progressive mismatch in alignment with respect to the DZ, within the MZ and the corresponding decrease in fiber alignment within the DZ may be an important imaging-based biomarkers for OA. Based on these findings it may be more appropriate to model collagen networks within healthy cartilage with the arcade model originally proposed by Benninghoff [7].

Table 1
Quantitative evolution of mean principal orientation θ, von Mises concentration parameter κ (as a measure of dispersion in orientation), and mean diameter plus IQR of collagen fibers in cartilage in health (H) and early grades of osteoarthritis (OA-0–OA-3), in the superficial zone (SZ), middle zone (MZ), and deep zone (DZ). Mean and 95% confidence interval (M±95%CI) are based on $n = 3-6$specimens within each zone-grade, assuming measurements within a grade-zone are normally distributed.

		Healthy	Grade 0	Grade 1	Grade 2	Grade 3
		($n = 3$)	($n = 3$)	($n = 6$)	($n = 3$)	($n = 3$)
Principal Orientation θ(radians, M±95%CI)	SZ	0.0447± 0.255	0.210±0.645	0.0777±0.107	0.286±0.631	0.320±0.382
	MZ	1.55±0.312	1.45±0.663	1.63±0.288	0.511±0.4875	1.36±0.442
	DZ	1.61±0.359	1.46±0.526	1.58±0.367	1.35±0.577	1.76±0.551
Concentration Parameter κ(–, M±95%CI)	SZ	7.32±14.4	1.55±1.54	3.46±1.55	2.22±1.49	1.13±0.430
	MZ	0.806±0.695	0.852±1.05	1.19±0.620	1.17±1.62	1.91±3.96
	DZ	1.42±0.844	2.45±0.894	1.67±1.20	1.22±1.54	1.56±2.13
Median Fiber Diameter (nm, M±95%CI)	SZ	41.1±19.3	38.1±4.41	39.1±10.4	38.1±5.22	35.8±14.3
	MZ	51.9±32.1	56.9±12.2	51.1±7.98	48.6±17.6	48.4±19.7
	DZ	61.9±44.7	59.6±53.8	67.8±13.8	60.0±19.3	65.3±15.9
Fiber Diameter IQR (nm, M±95%CI)	SZ	15.2±13.2	13.2±7.06	17.3±6.38	14.8±3.62	16.6±13.0
	MZ	28.1±22.8	31.9±19.2	26.8±6.30	21.4±6.44	23.3±11.8
	DZ	41.2±32.6	48.4±56.7	46.2±9.77	42.2±12.6	40.5±15.9

We observed relatively small diameter fibers ($\sim 25-125$ nm) in all three through-thickness zones, with larger diameter fibers (> 150 nm) appearing in the DZ, consistent with previous studies [3,15]. Using 10 nm wide bins to generate histograms we found that all zone-specific distributions of diameters of fibers are non-normal and right skewed. Conversely, previous studies reported bimodal distributions in histograms of fiber diameter [4,27].

4.2. Evolution of collagen morphology

We provided detailed measurements identifying morphological turning points in the progression of OA. We selected the OARSI grading method to quantify disease progression as it was designed to distinguish among early severities of OA. Our results show a general decrease in fiber alignment in the SZ with the progression of OA, consistent with previous studies highlighting increased disorganization of fibers with progression of OA [10,13]. The SZ, where collagen damage generally first presents, had the greatest change in dispersion during early OA [41,42]. The SZ exhibits structural differences even between healthy and grades zero and one, indicating changes in collagen microstructures possibly due to microscopic, metabolic changes of early OA. The large SE of κ for the SZ indicates alignment with the SLD can be very strong in regions of healthy cartilage [30]. Loss of tissue volume at the articular surface of cartilage during OA may disrupt the thickness-based calculation of zonal location for imaging the SZ. However, we found no significant differences in specimen thicknesses across OARSI grades $0-3$ in our study that would indicate substantial loss of SZ (data not shown) [43].

Our results support the current understanding of zonal fiber diameter distributions in health. While fibers larger than 200 nm become less abundant with the progression of OA, the lack of additional differences in distributions of fiber diameters either points to an otherwise stable network or removal of damaged fibers/fibrils. *In vitro* studies on chondrocyte metabolism have shown that collagen fragments in the extracellular matrix can induce production of metalloproteinases, possibly facilitating degradation of damaged collagen [44,45]. In the literature, reported observations on the evolution of fiber diameter with progression of OA were inconsistent. Some sources reported general and zonal decreases in fiber diameters with OA [15,27] while others observed significantly larger diameters [46]. Differences reported among previous studies may result from differences in experimental preparation and location (hip vs. knee). Here we focused on experimental consistency in an effort to reduce the number of confounding variables.

4.3. Inter- and intra-patient variability

Supported by our findings on inter-patient and inter-specimen variability, we assumed normality between specimens to estimate our reported parameters, cf. Table 1. We anticipated that there would be greater variability across grades than within specimens of the same grade from the same individual, and this was confirmed in our results. When modeling cartilage, e.g. with finite element analyses, inter- and intra-patient variability help determine the appropriateness of generalized model parameters and conclusions versus patient-specific methods.

4.4. Limitations and outlook

We made every attempt to accurately assess the morphology of the fiber network such that our results quantify the networks of collagen *in vivo*. Although we consistently applied a procedure designed to gently and uniformly dehydrate soft tissues without shifting collagen fibers, processing cartilage may alter the geometry [47]. Additionally, we captured all images in the plane parallel to the SLD while cartilage is three-dimensional. We assumed that the fiber networks all have one local principal orientation, where perhaps multiple principal orientations may better fit the data.

Our determination of the principal orientation was also susceptible to other imaging details. We designed the EM protocol to clear away all of the proteoglycans during dehydration, but it is possible some molecules remained and disrupted the contrast between the clear resin background and the solid collagen fibers. The collagen fibers were also densely packed in healthy and grade 0 cartilage of the SZ, potentially masking high alignment. With progression of OA tissue degeneration and swelling leads to greater spacing between fibers and thus more edges for detecting directionality.

Our morphological parameters characterizing individual specimens were well supported statistically and we obtained sufficient power in our analyses of zone effects. However, we were not able to distinguish the effects of grade versus anomalies in specific specimens perhaps due to our number of specimens per grade ($n \geq 3$) which also impacted the power of our analyses with lower effect sizes, e.g. grade effect on fiber diameters and κ mean in the DZ. Additionally, we assumed linear changes in network morphology when making grade a continuous fixed variable (the simplest assumption), while the progression of OA may not be linearly related to OARSI grade. Finally, although our fair interobserver agreement is a limitation, the number of independent observers provides support to our OARSI grading [48].

We provide the research community with *quantitative* data (1) on the through-thickness morphology of collagen in healthy cartilage and (2) on the evolution of through-thickness morphology of collagen with increasing histological grades of OA. Combining these results with results from studies on the depth-dependent and bulk mechanics of cartilage, e.g. Maier et al. [26, 49, 50], will also aid in understanding the intra-tissue mechanics of cartilage and its manifestations at the tissue level and through the progression of OA. Such understanding may

facilitate identifying image-based biomarkers and treatment targets, and ultimately finding clinical interventions for OA. Our quantitative results (measured parameters) also provide data for calibrating and/or validating models of OA degeneration, e.g. via finite element analyses.

Author contributions

PS contributed to conception and design; prepared specimens and conducted the experiments; analyzed and interpreted data; participated in drafting the article and revising it critically; and gave final approval of the version submitted. MBL contributed to development of image analysis protocol; participated in revising the article critically; and gave final approval of the version submitted. NCE contributed to the statistical analysis and interpretation; participated in revising the article critically; and gave final approval of the version submitted. CGL provided human tissues; participated in revising the article critically; and gave final approval of the version submitted. DMP oversaw the project; contributed to conception and design; analyzed and interpreted data; participated in drafting the article and revising it critically; and gave final approval of the version submitted.

Role of the funding source

Any opinions, findings, and conclusions or recommendations expressed in this material are those of the author(s) and do not necessarily reflect the views of the National Science Foundation or the U.S. Department of Education.

Conflict of interest

We have no conflicts of interest to report.

Acknowledgments

We thank the National Science Foundation 1662429 and U.S. Department of Education GAANN P200A160323 for funding. We thank the Musculoskeletal Transplant Foundation and the orthopedic surgeons of Hartford Healthcare Bone & Joint Institute for human tissues. We thank the Biosciences Electron Microscopy Facilities of the University of Connecticut, particularly Maritza Abril, Linnea Ostroff, and Xuanhao Sun for guidance. We also thank Franz Maier and Lauren Marshall for assistance with OARSI grading, and Nicole Madrid and Julie-Ann Williams for their assistance with image analyses.

Appendix A

In Figure A4 we provided results from our preliminary study on the sensitivity of our image analyses, where we ran the analyses at all possible ROI sizes.

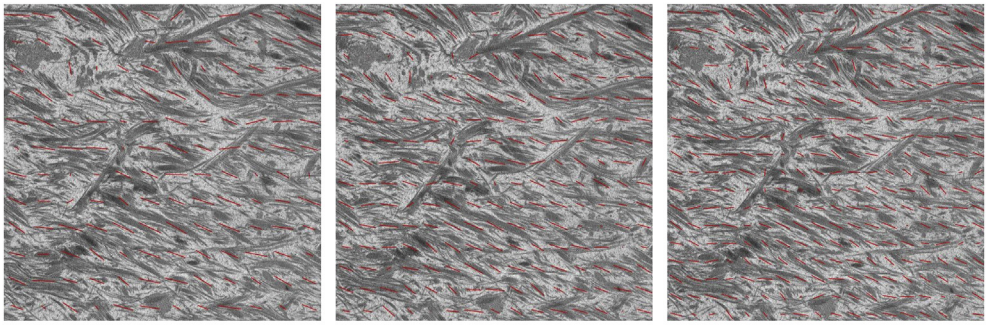

(a) $n = 12$ (b) $n = 15$ (c) $n = 18$

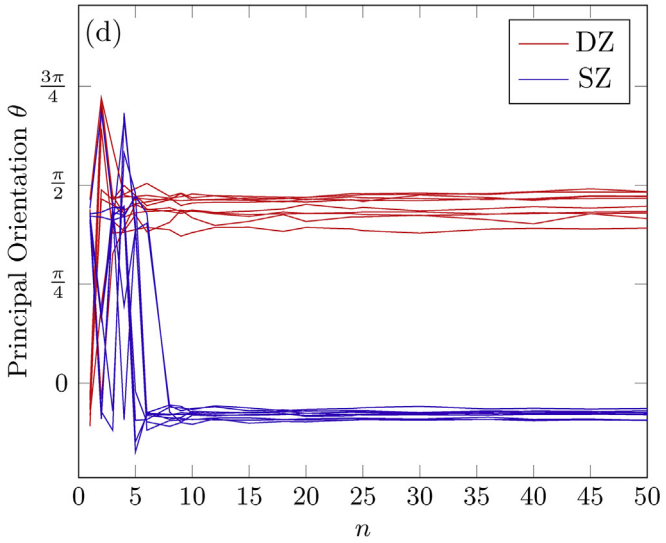

(e)

n	θ
9	1.21
10	1.22
12	1.23
15	1.24
18	1.24
20	1.22
24	1.22

Fig. A4. Preliminary study on the sensitivity of our image analyses. (a-c) Representative images presenting the principal orientations determined using $n \times n$regions of interest (ROIs) for $n = 12, 15, 18$respectively. (d) The mean principal orientation determined with our analyses stabilizes with sufficient resolution in ROIs, where images from the superficial zone (blue lines) present mean principal orientations parallel to the articulating surface ($\theta \approx 0$) and where images from the deep zone (red lines) present mean principal orientations perpendicular to the surface ($\theta \approx \pi/2$). (e) For $n \geq 9$. Changing the size of ROIs for subseque analyses, does not change the estimated principal orientation in a physically significant way (results from a representative image).

Appendix B

In Table B2 we provided a detailed summary of all specimens used for statistical analyses, including patient number and OARSI grade.

Table B2
Summary of patient source and OARSI grade for all 18 specimens used in this study. We extracted 30 pairs of specimens from eight patients and evaluated their OARSI grades. After reviewing the source of each and the corresponding histological assessment, we selected specimens to process for TEM imaging to determine effects of patient and grade on parameters quantifying the collagen networks. We included additional specimens in Grade 1 to investigate multiple specimens from the same grade and from the same patient.

Patient	Healthy	Grade 0	Grade 1	Grade 2	Grade 3	Total
1			1	1	2	4
2		1		1	1	3
3			2			2
4		1		1		2
5		1	3			4
6	1					1
7	1					1
8	1					1
Total	3	3	6	3	3	18

Appendix C

In Figure C5 we assumed a linear model for the change in zone-specific concentration parameter κ with the progression of osteoarthritis (OA) from healthy (H) to OARSI grade 3 (OA-3).

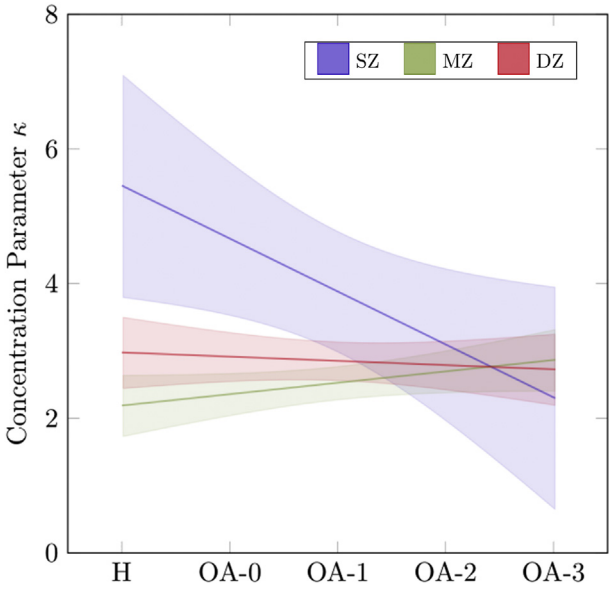

Fig. C5. Linear model and 95% confidence interval for the change in zone-specific concentration parameter κ with the progression of osteoarthritis (OA) from healthy (H) to Osteoarthritis Research Society International (OARSI) grade 3 (OA-3), where SZ = Superficial Zone, MZ = Middle Zone, and DZ = Deep Zone.

Appendix D

In Figure D6 we show representative results from a Grade 3 specimen for comparison to results from a Grade 0 specimen (Fig. 2).

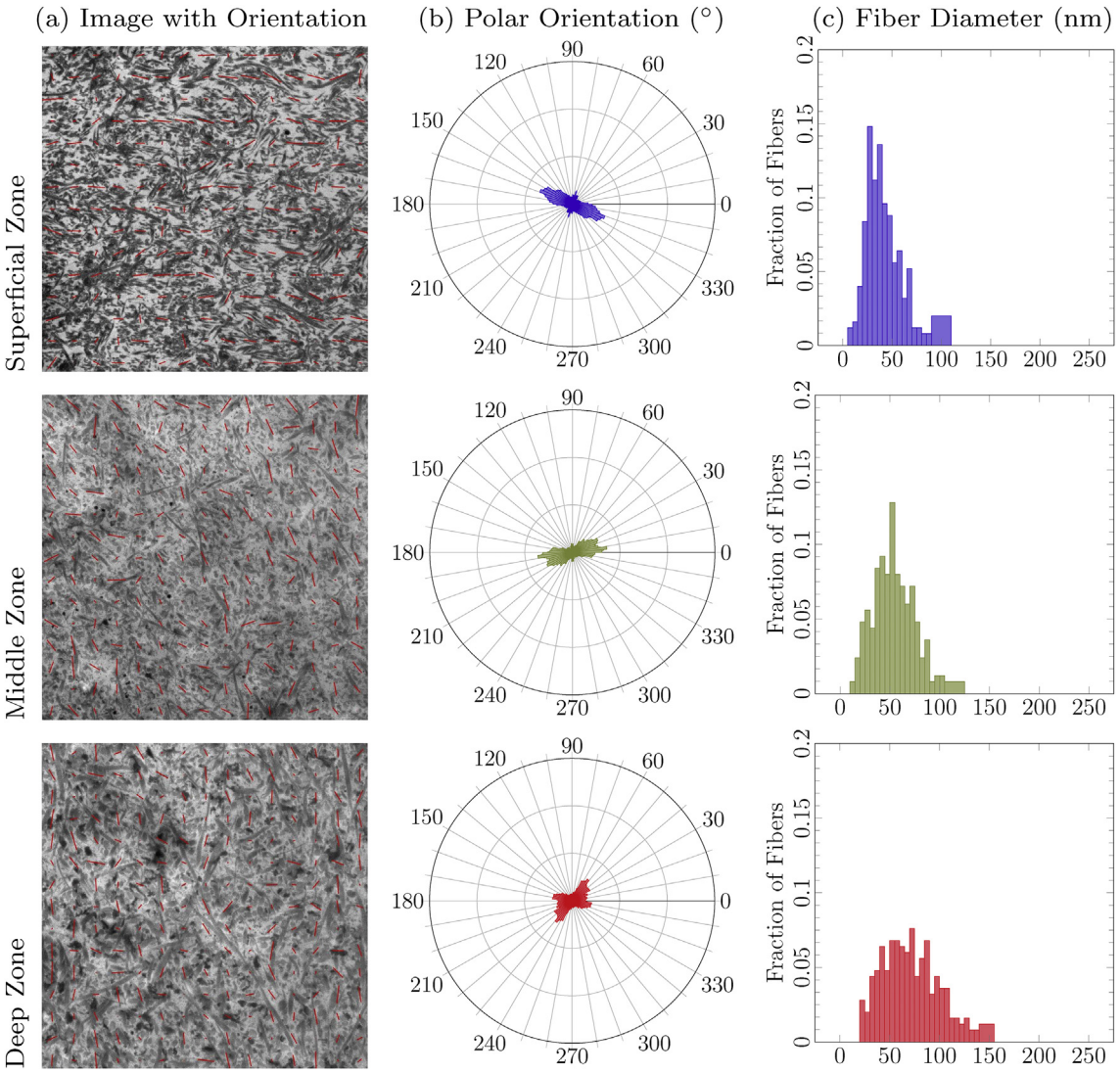

Fig. D6. Representative results from a cartilage specimen of Grade 3 show differences in principal orientation, dispersion in orientation, and diameter of fibers with representative results from a specimen of Grade 0 (Fig. 2) and between through-thickness zones. (a) Zonal images from transmission electron microscope (width = 6 μm) each reveal a different distribution of local principal directions within 225 ROIs, each represented as red vectors. (b) Corresponding probability-normalized polar histogram of principal orientation presented. (c) Corresponding histogram of diameter of fibers.

References

[1] N.D. Broom, D.L. Marra, Ultrastructural evidence for fibril-to-fibril associations in articular cartilage and their functional implication, J. Anat. 146 (1986) 185–200.
[2] W.B. Zhu, V.C. Mow, T.J. Koob, D.R. Eyre, Viscoelastic shear properties of articular cartilage and the effects of glycosidase treatments, J. Orthop. Res. 11 (1993) 771–781.
[3] A.J.S. Fox, A. Bedi, S.A. Rodeo, The basic science of articular cartilage: structure, composition, and function, Sport Health 1 (2009) 461–468.
[4] D.A.D. Parry, G.R.G. Barnes, A.S. Craig, A comparison of the size distribution of collagen fibrils in connective tissues as a function of age and a possible relation between fibril size distribution and mechanical properties, Proc. R. Soc. Lond. B 203 (1978) 305–321.
[5] J.L. Silverberg, S. Dillavou, L. Bonassar, I. Cohen, Anatomic variation of depth-dependent mechanical properties in neonatal bovine articular cartilage, J. Orthop. Res. 31 (2013) 686–691.
[6] V.C. Mow, W.Y. Gu, F.H. Chen, Structure and function of articular cartilage and meniscus, in: V.C. Mow, R. Huiskes (Eds.), Basic Orthopaedic Biomechanics & Mechano-Biology, third ed., Lippincott Williams & Wilkins, Philadelphia, 2005, pp. 181–258.
[7] A. Benninghoff, Form und Bau der Gelenkknorpel in ihren Beziehungen zur Funktion. II. Der Aufbau des Gelenkknorpels in seinen Beziehungen zur Funktion, Zeitschrift für Zellforschung und mikroskopische Anatomie 2 (1925) 783–862.
[8] G.E. Kempson, H. Muir, C. Pollard, M. Tuke, The tensile properties of the cartilage of human femoral condyles related to the content of collagen and glycosaminoglycans, Biochim. Biophys. Acta 297 (1973) 456–472.
[9] C. Huang, A. Stankiewicz, G.A. Ateshian, V. Mow, Anisotropy, inhomogeneity, and tension-compression nonlinearity of human glenohumeral cartilage in finite deformation, J. Biomech. 38 (2005) 799–809.
[10] J. Mansfield, V. Mandalia, A. Toms, C.P. Winlove, S. Brasselet, Collagen reorganization in cartilage under strain probed by polarization sensitivity second harmonic generation microscopy, J. R. Soc. Interface 16 (2018).
[11] H. Muir, P. Bullough, A. Maroudas, The distribution of collagen in human articular cartilage with some of its physiological implications, J. Bone Joint Surg. 52 (1970) 554–561.
[12] S. Henzgen, P.K. Petrow, K. Thoss, R. Braur, Degradation of articular cartilage during the progression of antigen-induced arthritis in mice: a scanning and transmission electron microscope study, Exp. Tox. Path. 48 (1996) 255–263.
[13] S. Saarakkala, P. Julkunen, P. Kiviranta, J. Mäkitalo, J.S. Jurvelin, R.K. Korhonen, Depth-wise progression of osteoarthritis in human articular cartilage: investigation of composition, structure and biomechanics, Osteoarthritis Cartilage 18 (2010) 73–81.
[14] R. Kumar, K.M. Grønhaug, C.L. Davies, J.O. Drogset, M.B. Lilledahl, Nonlinear optical microscopy of early stage (ICRS Grade-I) osteoarthritic human cartilage, Biomed. Opt. Express 6 (2015) 1895–1903.
[15] R. Gottardi, U. Hansen, R. Raiteri, M. Loparic, M. Düggelin, D. Mathys, N.F. Friederich, P. Bruckner, M. Stolz, Supramolecular organization of collagen

fibrils in healthy and osteoarthritic human knee and hip joint cartilage, PLoS One 11 (2016), e0163552.
[16] K.P. Quinn, I. Georgakoudi, Rapid quantification of pixel-wise fiber orientation data in micrographs, J. Biomed. Opt. 18 (2013).
[17] Z. Li, S. Qiu, S. Wu, H. Li, Quantification of collagen fiber orientation based on center line of second harmonic generation image for naturally aging skins, Opt. Lett. 14 (2018) 306–310.
[18] Y. Xia, K. Elder, Quantification of the graphical details of collagen fibrils in transmission electron micrographs, J. Microsc. 204 (2001) 3–16.
[19] M.B. Lilledahl, D.M. Pierce, T. Ricken, G.A. Holzapfel, C.L. Davies, Structural analysis of articular cartilage using multiphoton microscopy: input for biomechanical modeling, IEEE Trans. Med. Imag. 30 (2011) 1635–1648.
[20] A.J. Schriefl, A. Reinisch, S. Sankaran, D.M. Pierce, G.A. Holzapfel, Quantitative assessment of collagen fiber orientations from 2d images of soft biological tissues, J. R. Soc. Interface 9 (2012) 3081–3093.
[21] E.E. Morrill, A.N. Tulepbergenov, C.J. Stender, R. Lamichhane, R.J. Brown, T.J. Lujan, A validated software application to measure fiber organization in soft tissue, Biomech. Model. Mechanobiol. 15 (2016) 1467–1478.
[22] J.K. Pijanka, P.P. Markov, D. Midgett, N.G. Paterson, N. White, E.J. Blain, T.D. Nguyen, H.A. Quigley, C. Boote, Quantification of collagen fiber structure using second harmonic generation imaging and two-dimensional discrete fourier transform analysis: application to the human optic nerve head, J. Biophot. 12 (2018).
[23] J.P. McLean, Y. Gan, T.H. Lye, D. Qu, H.H. Lu, C.P. Hendon, High-sped collagen fiber modeling and orientation quantification for optical coherence tomography imaging, Opt 27 (2019) 14457–14471.
[24] M. Sun, A.B. Bloom, M.H. Zaman, Rapid quantification of 3d collagen fiber alignment and fiber intesection correlations with high sensitivity, PLO 10 (2015).
[25] C. Neu, A. Reddi, K. Komvopoulous, T. Schmid, P.D. Cesare, Friction coefficient and superficial zone protein are increased in patients with advanced osteoarthritis, Arthritis Rheum. 62 (2010) 2680–2687.
[26] F. Maier, C.G. Lewis, D.M. Pierce, The evolving large-strain shear responses of progressively osteoarthritic human cartilage, Osteoarthritis Cartilage 27 (2019) 810–822.
[27] A. Changoor, M. Nelea, S. Méhot, N. Tran-Khanh, A. Chevrier, A. Restrepo, M.S. Shive, C.D. Hoemann, M.D. Buschmann, Structural characteristics of the collagen network in human normal, degraded and repair articular cartilages observed in polarized light and scanning electron microscopies, Osteoarthritis Cartilage 19 (2011) 1458–1468.
[28] K.P.H. Pritzker, S. Gay, S.A. Jimenez, K. Ostergaard, J.-P. Pelletier, P.A. Revell, D. Salter, W.B. van den Berg, Osteoarthritis cartilage histopathology: grading and staging, Osteoarthritis Cartilage 14 (2006) 13–29.
[29] M. Szarko, K. Muldrew, J.E.A. Bertram, Freeze-thaw treatment effects on the dynamic mechanical properties of articular cartilage, BMC Muscoskel. Disord. 11 (2010).
[30] S. Below, S.P. Arnoczky, J. Dodds, C. Kooima, N. Walter, The split-line pattern of the distal femur: a consideration in the orientation of autologous cartilage grafts, Arthroscopy 18 (2002) 613–617.
[31] D.R. Keene, S.F. Tufa, Transmission electron microscopy of cartilage and bone, Methods Cell Biol. 96 (2010) 443–473.
[32] E. Batschelet, Circular Statistics in Biology - (Mathematics in Biology), Academic Press, London, England, 1981.
[33] N.I. Fisher, Statistical Analysis of Circular Data, Cambridge University Press, Melbourne, Australia, 1993.
[34] C.A. Schneider, W.S. Rasband, K.W. Eliceiri, Nih image to imagej: 25 years of image analysis, Nat. Methods 9 (2012) 671–675.
[35] R.L. Wasserstein, N.A. Lazar, The asa statement on p-values: context, process, and purpose, Am. Statist. 70 (2) (2016) 129–133, https://doi.org/10.1080/00031305.2016.1154108, arXiv:.
[36] D.F. Holmes, K.E. Kadler, The 10+4 microfibril structure of thin cartilage fibrils, PNAS 103 (2006) 17249–17254.
[37] S. Bancelin, C. Aimé, I. Gusachenko, L.K.G. Latour, T. Coradin, M. Schanne-Klein, Determination of collagen fibril size via absolute measurements of second-harmonic generation signals, Nat. Commun. 5 (2014).
[38] I. Redler, V.C. Mow, M.L. Zimny, J. Mansell, The ultrastructure and biomechanical significance of the tidemark of articular cartilage, Clin. Orthop. Relat. Res. 112 (1975) 357–362.
[39] C. Weiss, L. Rosenberg, A.J. Helfet, An ultrastructural study of normal young adult human articular cartilage, J. Bone Joint Surg. 50 (1968) 663–674.
[40] S. Zheng, Y. Xia, The collagen fibril structure in the superficial zone of articular cartilage by μMRI, Osteoarthritis Cartilage 17 (2009) 1519–1528.
[41] A.P. Hollander, I. Pidoux, A. Reiner, C. Rorabeck, R. Bourne, A.R. Poole, Damage to type II collagen in aging and osteoarthritis starts at the articular surface , originates around chondrocytes , and extends into the cartilage with progressive degeneration, J. Clin. Invest. 96 (1995) 2859–2869.
[42] F. Nelson, L. Dahlberg, S. Laverty, A. Reiner, I. Pidoux, M. Ionescu, G.L. Fraser, E. Brooks, M. Tanzer, L.C. Rosenberg, P. Dieppe, A.R. Poole, Evidence for altered synthesis of type ii collagen in patients with osteoarthritis, J. Clin. Invest. 102 (1998) 2115–2125.
[43] L. Hartlev, R. Klose-Jensen, J. Thomsen, L. Boel, M. Laursen, T. Laurberg, A. Nielsen, K. Steengaard-Pedersen, E. Hauge, Thickness of the bone-cartilage unit in relation to osteoarthritis severity in the human hip joint, RMD Open 4 (2018), e000747.
[44] L. Jennings, L. Wu, K.B. King, H. Hämmerle, The effects of collagen fragments on the extracellular matrix metabolism of bovine and human chondrocytes, Connect. Tissue Res. 42 (2001) 71–86.
[45] M. Fichter, U. Körner, J. Schömburg, L. Jennings, A.A. Cole, J. Mollenhauser, Collagen degradation products modulate matrix metalloproteinase expression in cultured articular cartilage, J. Orthop. Res. 24 (2006) 63–70.
[46] S. Maniwa, N. Maeki, H. Ishihara, Y. Takami, T. Tadenuma, Y. Sakai, Diameter of collagen fibrils in the superficial layer of osteoarthritic articular cartilage from different species, Osteoarthritis Cartilage 27 (2019) S148–S149.
[47] E.B. Hunziker, K. Lippuner, N. Shintani, How best to preserve and reveal the structural intricacies of cartilaginous tissue, Matrix Biol. 39 (2014) 33–43.
[48] J. Sim, C. Wright, The kappa statistic in reliability studies: use, interpretation and sample size requirements, Pharmacol. Ther. 3 (2005) 257–268.
[49] F.S. Maier, H. Drissi, D.M. Pierce, Shear deformations of human articular cartilage: certain mechanical anisotropies apparent at large but not small shear strains, J. Mech. Beh. Biomed. Mat. 65 (2017) 53–65.
[50] F. Maier, C.G. Lewis, D.M. Pierce, Through-thickness patterns of shear strain evolve in early osteoarthritis, Osteoarthritis Cartilage 27 (2019) 1382–1391.